Subunit Stoichiometry of Human Muscle Chloride Channels

Christoph Fahlke,[*‡] Timothy Knittle,[*‡] Christina A. Gurnett,[§‖] Kevin P. Campbell,[§‖] and Alfred L. George, Jr.[*‡]

From the *Department of Medicine and ‡Department of Pharmacology, Vanderbilt University School of Medicine, Nashville, Tennessee 37232; and §Howard Hughes Medical Institute and ‖Department of Physiology and Biophysics, University of Iowa College of Medicine, Iowa City, Iowa 52242

ABSTRACT Voltage-gated Cl^- channels belonging to the ClC family appear to function as homomultimers, but the number of subunits needed to form a functional channel is controversial. To determine subunit stoichiometry, we constructed dimeric human skeletal muscle Cl^- channels in which one subunit was tagged by a mutation (D136G) that causes profound changes in voltage-dependent gating. Sucrose-density gradient centrifugation experiments indicate that both monomeric and dimeric hClC-1 channels in their native configurations exhibit similar sedimentation properties consistent with a multimeric complex having a molecular mass of a dimer. Expression of the heterodimeric channel in a mammalian cell line results in a homogenous population of Cl^- channels exhibiting novel gating properties that are best explained by the formation of heteromultimeric channels with an even number of subunits. Heteromultimeric channels were not evident in cells cotransfected with homodimeric WT-WT and D136G-D136G constructs excluding the possibility that functional hClC-1 channels are assembled from more than two subunits. These results demonstrate that the functional hClC-1 unit consists of two subunits.

KEY WORDS: chloride channel • skeletal muscle • myotonia • subunit stoichiometry • electrophysiology

INTRODUCTION

The ClC family of voltage-gated Cl^- channels has recently been identified through molecular cloning (Jentsch et al., 1990; Jentsch, 1994), and several distinct mammalian ClC isoforms have been implicated in various cellular functions (Steinmeyer et al., 1991; Thiemann et al., 1992; Uchida et al., 1993; Adachi et al., 1994; Fisher et al., 1994; Kawasaki et al., 1994; Kieferle et al., 1994; van Siegtenhorst et al., 1994; Malinowska et al., 1995). Members of this class of proteins share no significant structural homology to other known ion channels, and are therefore likely to have unique properties concerning subunit stoichiometry, gating, and permeation mechanisms.

Several lines of evidence suggest that the functional ClC channel unit is composed of multiple identical components. Based upon detailed analyses of single *Torpedo* electroplax Cl^- channels reconstituted into planar lipid bilayers, Miller and colleagues proposed the "double-barreled shotgun" model to explain the occurrence of two equally spaced and independently gated subconductance states (Miller, 1982; Hanke and Miller, 1983; Miller and White, 1984). In this model the *Torpedo* channel consists of two identical ion conduction pathways or protochannels which are gated simultaneously by a common slow gate, but each protochannel is gated independently by a faster process. Examination of single channel recordings of cloned *Torpedo* Cl^- channels (ClC-0) expressed in *Xenopus* oocytes show that these distinct gating and conduction properties are completely reconstituted in a heterologous system indicating that a single cDNA is sufficient to code for this channel behavior (Bauer et al., 1991). These functional attributes of ClC-0 do not provide direct structural information about the subunit composition of the channel. However, a recent biochemical study of purified *Torpedo* Cl^- channels demonstrated that the native configuration of the protein has the sedimentation properties of a homodimer (Middleton et al., 1994).

Although it is natural to expect that all ClC channels will have similar multimeric structures, there is evidence in conflict with the biochemical data on ClC-0 that points toward tetrameric assembly of the skeletal muscle channel, ClC-1. This information has emerged from the functional characterization of naturally occurring mutations in a dominant form of congenital myotonia (Thomsen's disease). In this work, co-expression experiments in *Xenopus* oocytes revealed that two disease-producing mutants (G230E, P480L) exert negative effects on the functional expression of the wild-type human skeletal muscle Cl^- channel (hClC-1) (Steinmeyer et al., 1994). Based upon RNA titration experiments in which wild-type and mutant transcripts were co-expressed in oocytes, Steinmeyer and colleagues

Address correspondence to Alfred L. George, Jr., S-3223 MCN, Vanderbilt University Medical Center, 21st Avenue South at Garland, Nashville, TN 37232-2372. Fax: 615-343-7156; E-mail: ageorge@mbio.mc.vanderbilt.edu

proposed that functional channels are composed of four identical subunits.

The subunit stoichiometry of *Shaker* and related mammalian potassium channels has been ascertained in part by the analysis of artificial multimeric channels in which subunits have been covalently linked together (Isacoff et al., 1990; Liman et al., 1992). This novel and informative approach requires the "tagging" of at least one subunit with a mutation that alters a specific functional property such as inactivation or toxin block. Such a strategy can now be applied to the determination of subunit stoichiometry of the human skeletal muscle Cl⁻ channel (hClC-1) by assembling multimeric constructs incorporating a mutation, D136G, that causes a profound disturbance in voltage-dependent gating (Fahlke et al., 1995). The distinct gating properties of wild-type (WT)[1] and mutant hClC-1 provide the necessary "tags" to allow recognition of heteromultimeric channels and to quantify the probable number of subunits required to form a functional channel. In this paper, we report the successful application of this method for examining the subunit stoichiometry of hClC-1, and find strong evidence that the channel is a functional dimer.

METHODS

Construction of hClC-1 Dimers

The plasmid pSP64T-hClC-1 (Fahlke et al., 1995) was modified using recombinant PCR mutagenesis (Higuchi, 1989) so that the terminal amino acid residue (leu-988) in the open reading frame of hClC-1 is followed by a 20 amino acid linker sequence (SPLH-PGLYPYDVPDYAISAV), a new stop codon, and the recognition sequence for EcoRI. The nucleotide sequence of this linker also contains an EagI site located 9 bp 5′ to the new stop codon. To construct this modified hClC-1, a 484-bp PCR product was amplified using pSP64T-hClC-1 as a template and the following primers: 2553F, 5′-GACCAGCATGGGGAAGCTCA-3′ (nucleotides [nt] 2553–2572); and the linker-primer, 5′-CCG GAA TTC CTA AAC GGC CGA AAT TGC ATA GTC AGG TAC GTC ATA AGG ATA TAG TCC AGG ATG TAG GGG TGA AAG GAT CAG TTC AT-3′ (containing nt 2951–2965 at the 3′ end). The amplified product was then purified with Qiagen PCR Spin columns (QIAGEN Inc., Chatsworth, CA), digested with Bsu36I (cleaves at nt 2730 of hClC-1) and EcoRI to give a 307-bp fragment which was subsequently ligated to Bsu36I/EcoRI digested pSP64T-hClC-1. The final construct (designated hClC-DT) was sequenced completely in the region modified by PCR to verify the inserted sequence and to identify recombinants without polymerase errors. Functional expression of this modified hClC-1 in oocytes was performed as previously described (Fahlke et al., 1995), and the characteristics of the modified channel were indistinguishable from the original wild-type hClC-1.

The WT–WT hClC-1 dimer construct was assembled in the mammalian expression vector pRc/CMV by ligating together the following restriction fragments: WT pRc/CMV-hClC-1, HindIII/BspHI (containing 76 bp of vector polylinker and nt 1–1395 of

[1]*Abbreviations used in this paper:* nt, nucleotide; WT, wild-type.

hClC-1); hClC-1-DT, BspHI/EagI (nt 1396–2965, linker); WT–hClC-1, NotI/XbaI (nt 1–2999); and pRc/CMV, HindIII/XbaI. Recombinants were screened by PstI digestion, and correct constructs were identified by the presence of a unique 780–bp fragment as well as the appearance of double intensity ethidium bromide–stained fragments derived from the duplicated cDNA sequence. The D136G-D136G dimer construct was assembled in a similar manner except that the HindIII/BspHI and NotI/XbaI fragments were derived from D136G (Fahlke et al., 1995). The presence of the mutant sequence and the absence of WT sequence in the final D136G-D136G construct was verified by Southern blot hybridization of PstI digested plasmid DNA using allele-specific oligonucleotide probes. The WT–D136G construct was made by substituting only the NotI/XbaI fragment with the corresponding segment from D136G. Similarly, the D136G–WT construct was made by substituting the HindIII/BspHI fragment with the corresponding segment from D136G. Final constructs were shown to have both WT and D136G sequences in appropriate regions using allele-specific hybridizations.

Cell Lines and Transient Transfections

HEK-293 cells (ATCC CRL 1573; American Type Culture Collection, Rockville, MD) stably transfected with pRc/CMV-hClC-1 and pRc/CMV-WT–WT were produced as previously described (Fahlke et al., 1995). Transient transfection of tsA201 (HEK-293 cells stably transformed with the SV40 large T antigen) was performed as described by Chahine et al. (1994) using 10–15 μg of plasmid DNA and 10–100 μg of salmon sperm DNA as carrier (Chahine et al., 1994). Transfection efficiencies ranged from 20 to 80% as judged by the proportion of cells expressing Cl⁻ currents. For cotransfection experiments, 10 μg of each WT or WT–WT and D136G or D136G–D136G plasmids were used without carrier DNA. Typically 48 h after transfection, cells were split into 35-mm culture dishes and investigated at least 3 h later. Cells in which current amplitude exceeded 10 nA were excluded from analysis.

Electrophysiology

Standard whole-cell recording (Hamill et al., 1981) was performed using an Axopatch 200A amplifier (Axon Instruments, Foster City, CA). Pipettes were pulled from borosilicate glass and had resistances of 0.5–0.9 MΩ. More than 80% of the series resistance was compensated by an analog procedure. The calculated voltage error due to series resistance was always <5 mV. No digital leakage and capacitive current subtraction were used. Currents were filtered with an internal 4-pole Bessel filter with 1, 2, or 5 kHz (−3 dB) and digitized with sampling rates which are at least five times the filter frequency using a Digidata AD/DA converter (Axon Instruments). Cells were clamped to 0 mV for at least 15 s between test sweeps.

The bath solution contained (in mM) 140 NaCl, 4 KCl, 2 CaCl₂, 1 MgCl₂, and 5 HEPES; the pipette solution contained (in mM) 130 CsCl, 2 MgCl₂, 5 EGTA, and 10 HEPES. All solutions were adjusted to a pH of 7.4 with CsOH (pipette solutions) or NaOH (bath solutions).

Data Analysis

Data were analyzed by a combination of pClamp (Axon Instruments) and SigmaPlot (Jandel Scientific, San Rafael, CA) programs. All data are shown as means ± SD.

The time course of current activation was fit with an equation containing either one exponential or a sum of two exponentials and a time-independent value (*d*) as follows: $I(t) = a_1 \exp(-t/\tau_1) [+ a_2 \exp(-t/\tau_2)] + d$. Activation was analyzed for potentials < 0 mV only. Instantaneous current amplitudes were measured 100

μs after the voltage step. To construct activation curves as shown in Figs. 6 and 7, the instantaneous current amplitude (normalized to its maximum value at a fixed potential of −105 mV) measured after 750 ms prepulses to different voltages (V) was plotted vs. the preceding potential as described previously (Fahlke et al., 1995; Fahlke et al., 1996). This plot yields the voltage dependence of the relative open probability, P_{open} at the end of the 750-ms pulses. The activation curves obtained in this manner were fit with a single Boltzmann and a voltage-independent value: $I(V) = Amp \cdot [1 + \exp([V - V_{0.5}]/k_V)]^{-1} + constant$.

Simulation of the superposed WT and D136G hClC-1 currents was done by adding scaled current traces obtained from measurements on HEK 293 cells stably expressing WT or D136G hClC-1 channels. Data shown in Fig. 1, A and C, were used for Fig. 3, C and D. Scaling factors were chosen to obtain identity of the simulated current amplitudes with the measured current amplitudes from the WT–D136G hClC-1 transfected cell at two different recording times: either immediately after the voltage step or at the end of the voltage step. For this purpose a set of two linear equations ($I_{WT-D136G}[t_i] = a \cdot I_{WT}[t_i] + b \cdot I_{D136G}[t_i]$, where t_i is either immediately after or at the end of the voltage step) was solved to obtain the scaling factors a and b. Simulated data represent the sum of the WT current trace scaled by the factor a and the D136G current trace scaled with the factor b. For Fig. 6, current traces from recordings shown in Fig. 7, A and E, were added in ratios given in legends.

Expression in Xenopus Oocytes

For expression of WT–D136G and D136G–WT in *Xenopus* oocytes, coding regions from both were subcloned into the plasmid vector pSP64T and RNA transcribed in vitro using SP6 RNA polymerase as described previously (Fahlke et al., 1995). Transcripts were quantified by absorbance measurement at 260 nm and checked for size and purity by denaturing agarose gel electrophoresis. Co-expression experiments were performed by microinjecting a mixture containing equal quantities (10–20 ng) of WT–D136G and D136G–WT RNA.

Expression was examined by a two-electrode voltage clamp using a Warner Instrument Corp. (Hamden, CT) oocyte clamp 7C-725B amplifier. As previously described, WT and D136G hClC-1 channels share a high affinity for 9-anthracene carboxylic acid (9-AC) (Fahlke et al., 1995). To correct for leakage and endogenous currents conducted by channels other than hClC-1, oocytes were perfused with ND 96 + 0.2 mM 9-AC after each recording. The blocking process was monitored by repetitive pulses from a holding potential of −30 to −125 mV (0.1 Hz). After reaching steady-state levels, the same pulse protocols were performed, and the current amplitudes recorded under these conditions were subtracted from the original recording. Only subtracted recordings were used for analysis. For the calculation of I_{ss}/I_{peak}, the peak current (I_{peak}) was measured immediately after settling of the capacitive transient, and the steady-state current (I_{ss}) was measured at the end of the test pulse (Fig. 8).

Western Blot Analysis

Dishes (100 mm) of tsA201 cells transiently transfected with either WT–D136G or D136G–D136G cDNAs were washed with ice-cold PBS (10 mM Na phosphate, 0.9% NaCl, pH 7.4) and scraped into 15-ml polypropylene tubes. Cell suspensions were centrifuged at 2,000 g for 5 min at 4°C, and the resultant cell were pellets resuspended in 5–10 ml of ice-cold lysis buffer (50 mM Tris, 150 mM NaCl, 5 mM EDTA, 1% Triton X-100, pH 7.5) containing freshly added protease inhibitors (5 mM PMSF, 5 mM *N*-ethylmaleimide, 1 mM benzamidine), and mixed on a rocking platform at 4°C for 20 min. The lysates were centrifuged at 5,000 g

for 15 min at 4°C, the pellets discarded, and the supernatants were used for SDS-PAGE and immunoblotting without further purification. Plasma membranes from confluent 100-mm dishes of HEK-293 cells stably expressing either WT–hClC-1 or the WT–WT dimer were prepared as described by Deal et al. (Deal et al., 1994). 3–10 μg of protein (protein concentration determined by a modified Bradford assay, Bio-Rad Corp., Richmond, CA) was solubilized momentarily at 25°C in SDS sample buffer containing 30 mM DTT before electrophoresis.

Protein samples were fractionated by SDS-PAGE electrophoresis on precast 4–15% polyacrylamide gradient gels (Bio-Rad Corp.) and electro-transferred to Immobilon PVDF membranes (Millipore Corp., Bedford MA) at 50 V for 18 h at 4°C. After transfer, membranes were placed in a blocking solution consisting of 5% nonfat dry milk in TBS-T (50 mM Tris base, 150 mM NaCl, 0.05% Tween-20, pH 7.5) overnight at 4°C, washed twice with TBS-T, and probed for 2 h at 25°C with a 1:100 dilution of an affinity-purified rabbit polyclonal antibody directed against the carboxyl-terminus of ClC-1 (Gurnett et al., 1995). The membrane was washed twice with TBS-T and incubated for 1 h at 25°C with a 1:10,000 dilution of goat anti–rabbit IgG conjugated to horseradish peroxidase (Sigma Chemical Co., St. Louis, MO). After several washes in TBS-T, immunoreactive proteins were detected by enhanced chemiluminescence (ECL; Amersham Corp., Arlington Heights, IL).

Sucrose Density Gradient Centrifugation

Plasma membrane protein (250–400 μg) from HEK 293 cells stably transfected with hClC-1 monomer or WT–WT dimer were solubilized in SB buffer (1% Triton X-100, 50 mM Tris, 12.5 mM MgCl₂, 1.5 mM EGTA, 150 mM NaCl, 1.0 mM PMSF, 3.0 mM benzamidine, 1.0 mM *N*-ethylmaleimide, pH 7.5) for 1 h at 4 Arlington Heights, ILC. The samples were centrifuged in a Beckman 70.1 ti rotor (Beckman Instruments, Inc., Fullerton, CA) at 100,000 g for 1 h at 4°C. The hClC-1 supernatants and standard proteins were loaded on separate, continuous 7.5–20% sucrose gradients prepared with SB buffer containing 0.1% Triton X-100, then centrifuged in a Beckman SW 40 ti rotor at 100,000 g for 16 h at 4°C. Individual gradients were fractionated bottom-to-top by dropwise collection into 32 tubes (8 drops, ≅ 370 μl). Aliquots (24 μl) were fractionated on 4–15% gradients SDS-PAGE gels and were analyzed either by silver staining (protein standards) or Western blotting (WT, WT–WT) as described above.

RESULTS

Expression of Tandem hClC-1 Constructs

Initially, to test the feasibility of expressing tandem Cl⁻ channels, we constructed a WT hClC-1 homodimer (WT–WT) by covalently coupling two complete hClC-1 coding sequences together in a single reading frame using a short (20 amino acid) hydrophilic linker. This linker was designed to have minimal predicted secondary structure similar to a linker peptide sequence used to create heteromultimeric potassium channels (Liman et al., 1992). Similarly, we constructed a homodimeric construct containing two mutant hClC-1 channels having the D136G substitution in the first transmembrane spanning segment. Both WT–WT and D136G–D136G constructs were assembled in the mammalian expression plasmid, pRc/CMV, and used to transfect HEK-293 or tsA201 cells. Expression of both homodimers

leads to very high expression levels with many cells exhibiting peak current amplitudes greater than 10 nA. For data analysis, only cells with current amplitudes within the range 1–10 nA were used.

Fig. 1 shows the results of whole-cell current recordings made in cells transfected with either monomeric (WT, D136G) or homodimeric (WT–WT, D136G–D136G) cDNA constructs. Cells expressing either WT or WT–WT exhibit rapid deactivation elicited with hyperpolarizing voltage steps from a holding potential of 0 mV that is characteristic of this channel (Steinmeyer et al., 1991; Pusch et al., 1994; Fahlke et al., 1996). Expression of D136G and D136G–D136G constructs resulted in currents which exhibit slow activation upon hyperpolarization as previously described (Fahlke et al., 1995). Current-voltage relationships and steady-state activation curves were identical between corresponding monomeric and dimeric channels (data not shown). These results indicate that the functional phenotypes of both WT and D136G are preserved in the homodimeric constructs, and that the artificial peptide linker has no effect on channel function.

Biochemical Characterization of hClC-1 Dimers

To verify that our tandem constructs did indeed encode dimeric proteins, we performed Western blot analyses on cells transfected with either WT, or one of the dimeric constructs (Fig. 2 *A*). Cells transfected with the monomeric WT channel express a single ~120–130

kD protein detectable by using an anti–ClC-1 antibody (Gurnett et al., 1995). Cells transfected with WT–WT, D136G–D136G, and WT–D136G (see below) all express a single protein having a molecular mass of ~240 kD indicating that our cDNA constructs encode dimeric proteins.

We also characterized the sedimentation properties of monomeric and dimeric hClC-1 by centrifugation through nondenaturing sucrose density gradients to estimate the molecular mass of the native channel complex. Fig. 2 *B* shows results from a representative experiment in which identical sucrose gradients were loaded with triton X-100 solubilized membranes from HEK-293 cells stably expressing either hClC-1 monomer or the WT–WT dimer. Identical 7.5–20% sucrose density gradients loaded with various purified protein molecular weight standards or HEK cell membranes were centrifuged simultaneously. Individual fractions from each gradient were electrophoresed on SDS-PAGE gels and subjected to either silver staining (molecular weight standards) or Western blotting (WT, WT–WT). The fractions containing the peak silver stained protein standards are plotted on the horizontal axis in Fig. 2 *B* to provide molecular mass references in the sucrose gradient. The fractions containing either WT hClC-1 monomers or WT–WT dimers were identified by immunodetection using polyclonal anti–ClC-1 antibody and these results are vertically aligned with the fraction number displayed on the horizontal axis. Both WT and WT–WT sediment to a level corresponding to the molecular weight range between aldolase (158 kD) and catalase (240 kD). Peak quantities of immunoreactive protein were observed in fractions 19–23 for the WT monomer, and fractions 19–21 for the WT–WT dimer. The slight difference in sedimentation properties of WT and WT–WT is small in comparison to the separation of the 158 and 240 kD reference proteins, and probably represents minor differences between individual gradients. No immunoreactive protein was detected in either the WT or WT–WT gradients above fraction 25 or below fraction 15. Similar results were obtained in two independent density gradient experiments (data not shown). These results indicate that the native configuration of both WT and WT–WT exhibit similar sedimentation properties in their nondenatured states consistent with formation of homomultimers of hClC-1. Furthermore, the approximate molecular weight of the native complex is within the range expected for a dimeric protein.
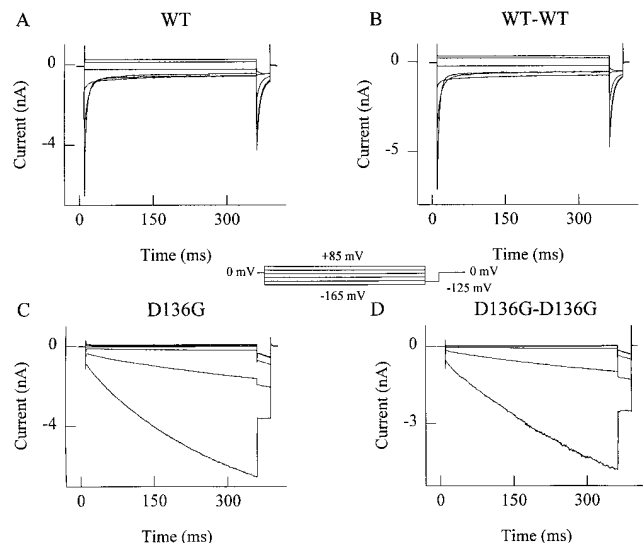

FIGURE 1. Expression of WT–WT and D136G–D136G homodimeric constructs. Responses to voltage steps from a holding potential of 0 mV to between −165 mV and +85 mV in 50-mV steps. Test pulses are followed by a voltage step to −125 mV. (*A*–*D*) Current recordings made from cells expressing either WT hClC-1 (*A*), the WT–WT dimeric construct (*B*), D136G hClC-1 (*C*), or the D136G–D136G dimeric construct (*D*).

Expression of Heterodimeric WT–D136G Channels

We combined WT and D136G together in a single reading frame as a tool to explore the functional subunit stoichiometry of hClC-1. Cells transiently transfected with the WT–D136G construct expressed large Cl⁻ cur-
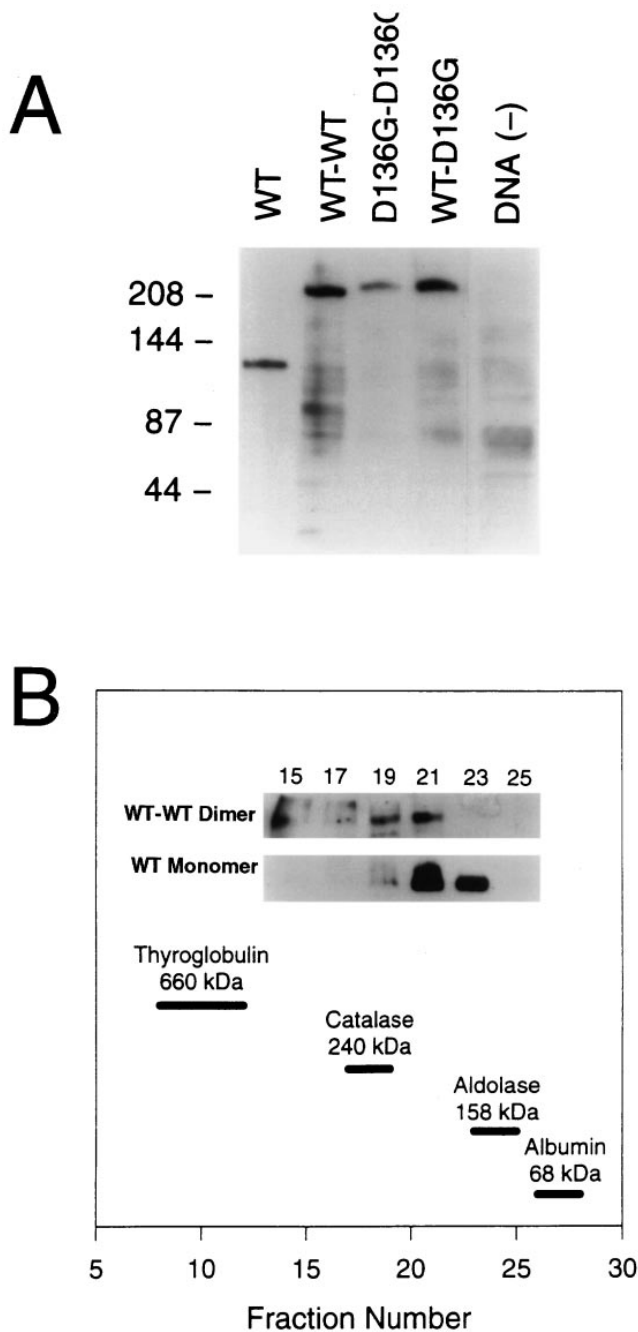
rents and synthesize a protein of molecular mass appropriate for an hClC-1 dimer (Fig. 2 A). Fig. 3 A shows representative whole-cell recordings made from cells transfected with WT–D136G. In contrast to D136G but similar to WT channels, WT–D136G cells express currents exhibiting rapid deactivation upon hyperpolarization. However, WT–D136G currents deactivate to an extent much less than WT channels. In WT–D136G-expressing cells, current measured 300 ms after onset of a -165 mV voltage-step ("steady-state" current) is approximately fivefold larger than it is for WT; the fractional steady-state currents were 0.47 and 0.1 for WT–D136G and WT, respectively. At -165 mV, WT–D136G currents also exhibit a very small ($<5\%$ of peak current) slowly activating component which is never seen in WT channels. The voltage dependence of the instantaneous as well as that of the current amplitude at the end of the test pulse displays inward rectification (data not shown). Thus, expression of WT–D136G gives rise to
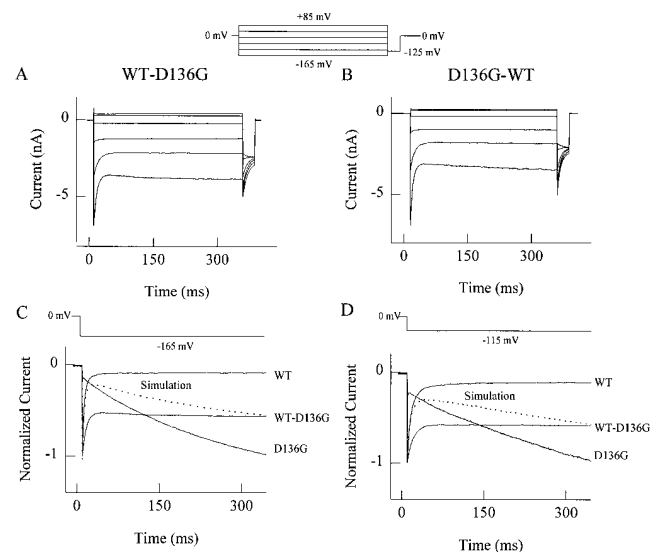
FIGURE 2. Biochemical characterization of hClC-1 dimers. (A) Western blot of recombinant hClC-1 constructs and sham transfected cells [DNA (–)]. The migration of molecular mass (in kD) standards are shown on the left of the panel. (B) Sucrose density gradient centrifugation experiment using WT and WT–WT hClC-1 constructs. The location of size standards are indicated by thick horizontal lines positioned above the corresponding fractions from the sucrose gradient. Inset: autoradiographs showing immunodetection of hClC-1 proteins in various gradient fractions (WT–WT dimer; WT monomer). Maximal immunoreactivity was seen in fractions 19–21 for WT–WT dimer, and 21–23 for WT monomer.

FIGURE 3. Properties of WT–D136G heteromultimeric hClC-1 channels. (A) Current recordings from a cell transiently transfected with the WT–D136G dimeric construct elicited with voltage steps to between -165 and $+85$ mV in 50-mV steps. Each voltage step is followed by a -125-mV test pulse. (B) Current recordings from a cell transiently transfected with the D136G–WT dimeric construct elicited with voltage steps to between -165 and $+85$ mV in 50-mV steps. Each voltage step is followed by a -125-mV test pulse. (C) Normalized current recordings from WT, WT–D136G, or D136G hClC-1 expressing cells at a test potential of -165 mV. The dotted lines represent the addition of WT and D136G current traces scaled such that the peak current amplitude and the amplitude at the end of the test step are identical to the normalized WT–D136G recording. (D) Normalized current recordings from WT, WT–D136G, or D136G hClC-1 expressing cells at a test potential of -115 mV. The dotted lines represent the addition of WT and D136G current traces scaled such that the peak current amplitude and the amplitude at the end of the test step are identical to the normalized WT–D136G recording.

Cl⁻ currents with gating properties distinct from either WT or D136G. We also considered that subunit order could be a factor in the genesis of the novel gating phenotype observed in WT–D136G expressing cells as was found in studies of tandem voltage-gated K^+ channels (McCormack et al., 1992), and therefore constructed a heterotandem construct with the reversed order of subunits (designated as D136G–WT). In cells transiently transfected with D136G–WT, we observed an identical gating phenotype as seen in WT–D136G expressing cells (Fig. 3 *B*).

To evaluate whether the current recordings made in WT–D136G expressing cells could result from a simple superimposition of the individual current components of WT and D136G, we compared these data with simulations of currents that would result from the addition of the two individual channels. The results of this simulation done at two voltages (-165 and -115 mV) were then compared to current recordings of the monomeric and heterodimeric channels. The simulated currents exhibit rapid deactivation followed by a large slowly activating component. In a qualitative manner, actual WT–D136G current recordings are obviously distinct from the simple sum of the two separate channels (Fig. 3, *C* and *D*). These data indicate that channels encoded by WT–D136G and D136G–WT are gated by a mechanism resulting from an interaction between the two covalently coupled subunits and are consistent with the formation of heteromultimeric channels. Furthermore, this subunit–subunit interaction is independent of the subunit order.

A quantitative analysis of the gating properties of Cl⁻ currents in WT–D136G transfected cells reveal that there is a homogenous population of channels present. Evidence for channel homogeneity comes from studies of the time course of activation. The time course of current activation elicited by depolarizing test potentials following a prepotential of -100 mV is shown for WT–D136G (Fig. 4 *A*), WT channels (Fig. 4 *B*), and D136G (Fig. 4 *C*). The time course for WT–D136G activation is well fit by a single exponential function, whereas WT

channel activation is biexponential and consists of fast and slow components. The activation time constants for WT–D136G and WT are not voltage-dependent in the negative potential range, and the mean value of the activation time constant for WT–D136G ($\tau = 7.7 \pm 1.4$ ms, $n = 4$) is not statistically different from the fast activation time constant for WT channels ($\tau_{fast} = 7.4 \pm 1.1$ ms, $n = 4$). The absence of a second exponential component in WT–D136G activation indicates that the contribution of homomultimeric WT channels (and by inference, homomultimeric D136G channels) is negligible. Homogeneity of the expressed current phenotype suggests that functional channel complexes are formed by an even number of subunits. If the channel complex were formed by an odd number of subunits, we would expect a mixed current phenotype because of unequal incorporations of mutant and WT subunits. These data also imply that a single mechanism simultaneously gates the ion pore or pores of hClC-1, although it is not possible to know the exact pore stoichiometry from our results. Based upon our results from the heterotandem expression experiments, we conclude that a cooperative interaction between an even number of at least two subunits is required to form functional hClC-1 channels.

Co-Expression of WT–WT and D136G–D136G Homodimers

We considered the various subunit configurations which might exist for channel complexes comprised of either two or four subunits and this is illustrated in Fig. 5. Because we cannot functionally distinguish between dimeric channels consisting of one or two identical pores (with a common gate), we have chosen to draw the ion pore as a shared structure in the two subunit configurations. For tetrameric channel assemblies, we have considered both one and two pore architectures. To help distinguish among these possible subunit configurations, we performed co-expression studies in which both WT–WT and D136G–D136G homodimers were introduced into the same cell. This was accomplished by cotransfecting tsA201 cells with equal quan-
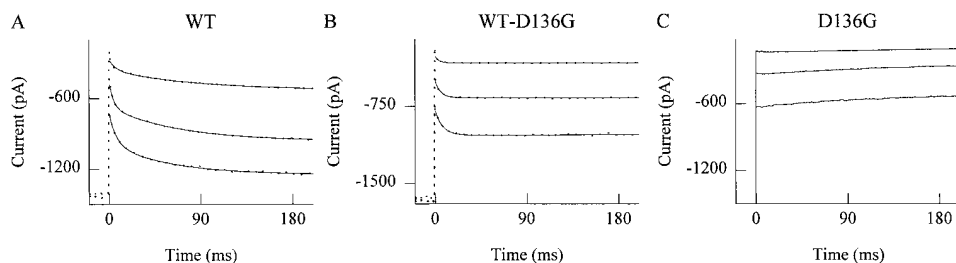

FIGURE 4. Homogenous gating properties of WT–D136G. Activation was examined in current recordings (*dotted lines*) elicited by voltage steps from -100 mV to between -65 and -25 mV in 20-mV steps for WT–hClC-1 (*A*), WT–D136G (*B*), and D136G (*C*). Solid lines represent fits with $I(t) = a_1 e^{-t/\tau 1} + a_2 e^{-t/\tau 2} + c$ in *A* and $I(t) = a_1 e^{-t/\tau 1} + c$ in *B* where a_1 and a_2 are amplitude terms and τ_1 and τ_2 are time constants. Currents shown for D136G are not fitted.

tities of each cDNA construct and then examining the cells for transient channel expression. We predicted that if the functional channel unit is composed of only two subunits, then co-expression of the two homodimers should result in a simple summation of the two current phenotypes of WT and D136G. If the channel is tetrameric, then WT homotetramers, D136G homotetramers, and WT–D136G heterotetramers should co-exist. The distinct gating properties of WT, D136G, and WT–D136G provide a tool to identify the presence of these three different channel configurations.

Fig. 6 shows representative current recordings made from three different cells cotransfected with WT–WT and D136G–D136G (Fig. 6, *A*, *C*, and *E*). In all cells, the currents exhibit rapid deactivation followed by a large slowly activating component, but there is heterogeneity among the cells with respect to the balance of the two current components. We explain the multiple current phenotypes by cell-to-cell variability in the relative expression levels of WT–WT and D136G–D136G. These three different current patterns strongly resemble the simple summation of WT and D136G phenotypes in varying proportions. Simulations reveal similar patterns of channel gating behavior with 5:1, 2:1, and 1:2 ratios of WT:D136G currents (Fig. 6, *B*, *D*, and *F*). These data provide qualitative evidence that WT–WT and D136G–D136G express independently, and that there is no formation of heteromultimeric channels in these experiments.
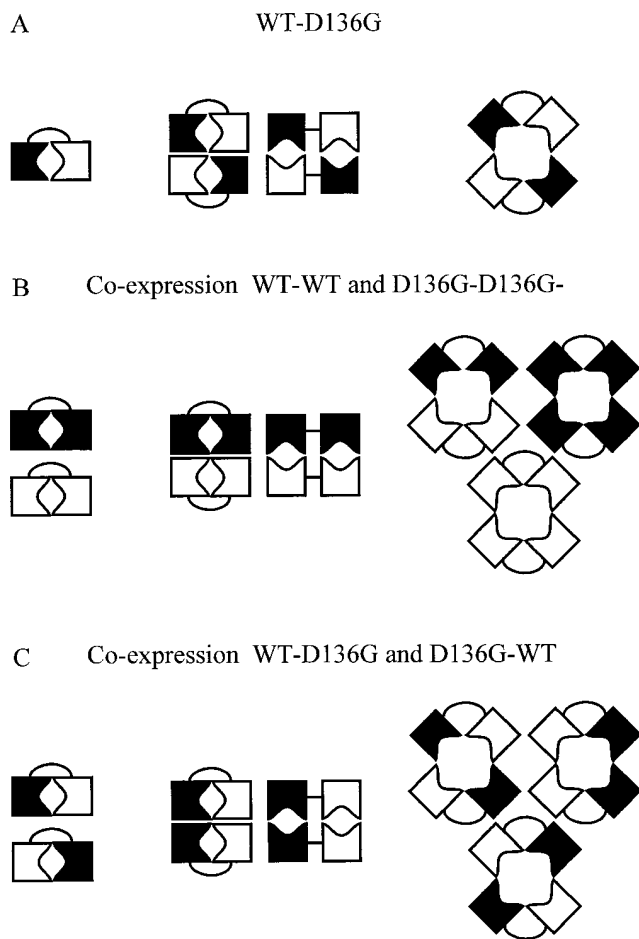

FIGURE 5. Possible configurations of heterodimeric and homodimeric hClC-1 channels. WT hClC-1 is illustrated by a black square and D136G by a white square. Each subunit has a single pore forming region indicated by the concave face. (*A*) Assembly of WT–D136G heterodimers into heterotetramers with either one or two pores is shown. (*B*) Assembly of tetrameric channels by the combination of WT–WT and D136G–D136G homodimers is shown. If hClC-1 is a tetramer, then homodimeric constructs would be expected to form a mixture of homotetrameric and heterotetrameric channels. (*C*) Assembly of WT–D136G and D136G–WT heterotandems into various tetrameric arrangements.
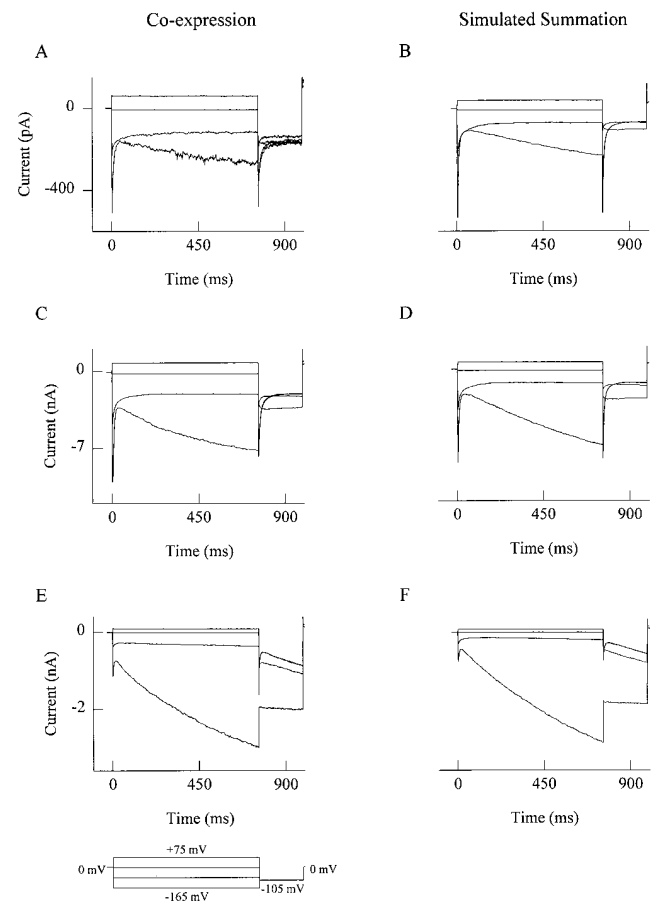

FIGURE 6. Cotransfection of WT–WT and D136G–D136G dimer constructs. (*A*, *C*, and *E*) Current recordings in cells cotransfected with equal quantities of WT–WT and D136G–D136G DNAs elicited with voltage steps to between −165 and +75 mV in 80 mV-steps from a holding potential of 0 mV. Each voltage step is followed by a fixed test pulse to either −105 mV (*A* and *C*) or −135 mV (*E*). (*B*, *D*, and *F*) Simulated current records of superimposed WT and D136G Cl⁻ currents in ratios of 5:1 (*B*), 2:1 (*D*), or 1:2 (*F*).

We exploited the distinct gating properties of WT, WT–D136G, and D136G as a tool to evaluate the subunit composition of the expressed channels using a more quantitative analysis. This was accomplished by subtracting the "pure" D136G component from the currents observed in co-transfection experiments, and determining if the residual current components resemble the pure WT phenotype or a mixture of WT and heteromultimeric channels. To accomplish this, we examined peak instantaneous and late currents resulting from a test pulse of −105 mV that is preceded by various prepotentials (Fig. 7). This is a similar pulse protocol used in Fig. 1 except our analyses were restricted to the "tail" portion of the records. Fig. 7 illustrates the results obtained from cells expressing WT, WT–D136G, or D136G alone to determine the essential characteristics of each channel with this pulse protocol (Fig. 7, *A*, *C*, and *E*). For both WT and WT–D136G, the current amplitudes measured at the end of the −105 mV test potential (I_{ss}) were the same for all prepotentials (i.e., are voltage independent, Fig. 7, *B* and *D*), whereas the D136G currents decrease with more depolarized prepotentials (Fig. 7 *F*). Therefore, a decrease of I_{ss} at the end of the −105 mV test potential can be used as a marker of pure D136G current. Furthermore, WT can be distinguished from WT–D136G by the ratio I_{ss}/I_{peak} determined at the most negative prepotential (WT: $I_{ss}/I_{peak} = 0.11 \pm 0.03$, $n = 5$; WT–D136G: $I_{ss}/I_{peak} = 0.48 \pm 0.06$, $n = 5$). Moreover, the voltage dependence of the normalized I_{peak} differs greatly between WT and WT–D136G; the voltage dependence of I_{peak} can be well fit with a single Boltzmann function for WT alone, but not for WT–D136G.

In Fig. 8, *A*, *B*, and *C*, we show the analysis of a representative cell cotransfected with both WT–WT and D136G–D136G. These data show a clear decrease in I_{ss} (*open squares*) between −165 and −85 mV. The slope of a straight line fit to the first four data points in Fig. 8 *B* was divided by the slope of a similar line fit to the data in Fig. 7 *F*. The ratio of these two slopes was used as a scaling factor to estimate the proportion of steady-state current in Fig. 8 *B* due to pure D136G channels. This value was obtained by multiplying the normalized current values in Fig. 7 *F* by the derived scaling factor and then subtracting these values at each prepotential from the data shown in Fig. 8 *B*. This subtraction gives the normalized current voltage relationship for the residual current component. Inspection of this residual component reveals its close similarity to the WT current-voltage relationship shown in Fig. 8 *C*, and the dependence of the instantaneous current amplitude on the prepulse potential can be fit with a single Boltzmann function and a constant term. The parameters of this fit in the WT–WT:D136G–D136G cotransfected cell are indistinguishable from values obtained from
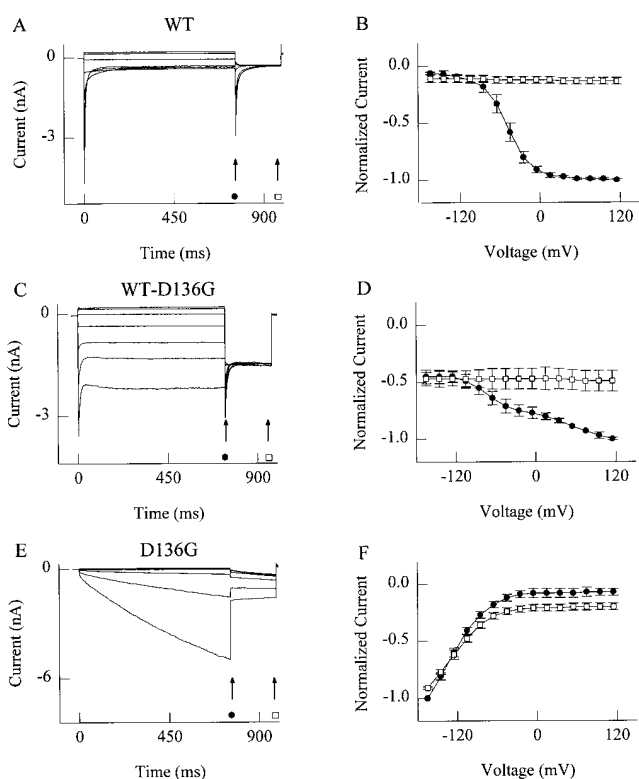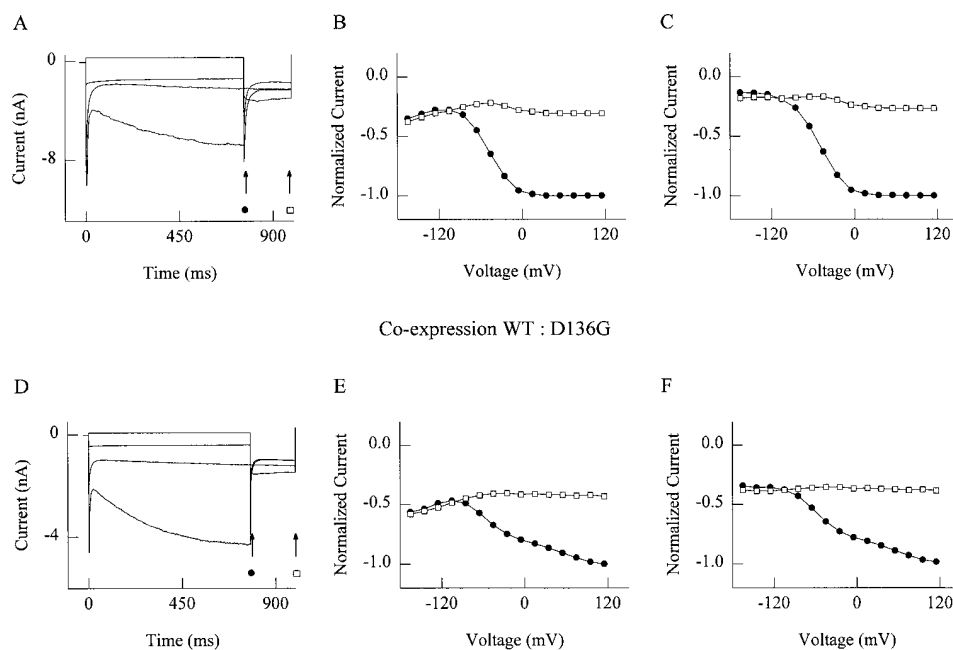

FIGURE 7. Activation curves for homomultimeric and heteromultimeric channels. (*A*, *C*, and *E*) Current responses to voltage steps between −165 mV and + 75 mV in 40-mV steps followed by a fixed test pulse to −105 mV. Measurements were performed on cells expressing either WT (*A*), WT–D136G (*C*), or D136G (*E*) channels. (*B*, *D*, and *F*) Voltage dependence of the normalized current amplitude measured either at the beginning (*filled circles*, I_{peak}) or at the end of (*open squares*, I_{ss}) the −105-mV test pulse for WT (*D*), WT- D136G (*E*), and D136G (*F*) channels. Each point represents mean ± SD ($n = 4$).

WT expressing cells ($V_{0.5} = -53.9 \pm 7.6$ vs. -51.1 ± 5.9 mV for WT, $n = 7$, $P > 0.1$; $k_V = -21.9 \pm 4.1$ vs. -18.9 ± 0.9 mV for WT, $n = 7$, $P > 0.1$). Furthermore, the I_{ss}/I_{peak} ratio determined at the most negative prepotential for the residual current component in WT–WT:D136G–D136G cotransfected cells was 0.13 ± 0.09 ($n = 9$) and is not significantly different from WT channels (0.11 ± 0.03, $n = 5$). It is therefore unlikely that this residual current has a component due to the formation of heteromultimeric channels. This analysis should be sufficiently sensitive to detect heteromultimeric channel phenotypes in the context of a tetrameric channel assembly. If the channel were a tetramer, then WT, heteromultimer, and D136G phenotypes would exist in proportions consistent with a binomial distribution. Even in the case of threefold lower expression levels of the D136G homodimer, a current component resulting from formation of heterotetramers should represent 37.5% of the total current (calculation based on a standard binomial distribution in which current pheno-

Co-expression WT-WT : D136G-D136G

Co-expression WT : D136G

FIGURE 8. Quantitative analysis of WT:D136G homodimer and monomer co-expression. (*A*) Current recordings from a cell cotransfected with WT–WT and D136G–D136G homodimer constructs. Responses to voltage steps between −165 and +115 mV in 40-mV steps are illustrated. Each voltage step is followed by a fixed −105-mV test pulse. (*B*) Voltage dependence of the instantaneous current amplitude (*filled circles*, I_{peak}) and the current amplitude at the end of the −105-mV test pulse (*open squares*, I_{ss}) in WT–WT:D136G–D136G cotransfected cells. (*C*) Current amplitudes shown in (Fig. 7 *C*) corrected for the contribution of Cl⁻ currents conducted by D136G homomultimeric channels as described in the text. (*D*) Current recordings from a cell cotransfected with WT and D136G monomer constructs. Responses to voltage steps between −165 and +15 mV in 60-mV steps are illustrated. Each voltage step is followed by a fixed −105-mV test pulse. (*E*) Voltage dependence of the instantaneous current amplitude (*filled circles*, I_{peak}) and the current amplitude at the end of the −105-mV test pulse (*open squares*, I_{ss}) in WT:D136G co-transfected cells. (*F*) Current amplitudes corrected for the contribution of Cl⁻ currents conducted by D136G homomultimeric channels as described in the text.

types would exist in the ratio of $a^2:2ab:b^2$, where a = WT–WT density, b = D136G–D136G density, a^2 = probability of forming WT homotetramers, b^2 = probability of forming D136G homotetramers, $2ab$ = probability of heterotetramer formation).

This quantitative analysis was able to detect the presence of heteromultimeric channels in an experiment where WT and D136G monomer constructs were cotransfected into tsA201 cells. Fig. 8, *D, E*, and *F*, show analysis of a representative WT:D136G co-expressing cell. In this cell, subtraction of pure D136G steady-state current leaves a residual component with an I_{ss}/I_{peak} ratio of 0.39. This I_{ss}/I_{peak} value is significantly larger than observed for WT alone or what was observed in the homodimer co-expression experiment and is intermediate between values observed for WT and WT–D136G. Furthermore, the voltage dependence of the subtracted I_{peak} cannot be fit with a single Boltzmann function consistent with more than one current component. Similar evidence for heteromultimeric channel formation was observed in all cells examined ($n = 7$). This experiment demonstrates the ability of this method to detect heteromultimeric current components and also helps exclude the possibility that WT and D136G subunits do not co-assemble unless covalently linked.

Co-Expression of WT–D136G and D136G–WT Heterodimers

The absence of a heteromultimeric current component in the co-transfection experiments with WT–WT and D136G–D136G excludes a tetrameric channel assembly with two pores (Fig. 5 *B*). In considering the various channel architectures shown in Fig. 5, we recognized the remote possibility that subunit arrangement in a single pore tetramer could be a factor in determining the gating phenotype. For example, assembly of one WT–WT dimer with one D136G–D136G dimer into a single pore tetramer having the identical subunits in adjacent positions gives rise to currents indistinguishable from either WT alone, D136G alone, or the linear sum of WT and D136G. However, we can evaluate this possibility by co-expressing WT–D136G with D136G–WT. If the channel is a single pore tetramer, then one would expect formation of two complexes in which the identical subunits are diagonally arranged (similar to the situation with WT–D136G alone) and one complex with the identical subunits in adjacent positions (Fig. 5 *C*). If the latter complex gives rise to WT, D136G, or summed current phenotypes, then we should observe one of these possibilities in addition to heteromultimeric channels. To test his idea, we expressed WT–D136G and D136G–WT simultaneously in oocytes and

measured current with the two-electrode voltage clamp. Oocytes were used in this experiment to better control the stoichiometry of channel expression. Expression of both WT–D136G and D136G–WT alone or in combination give rise to identical current phenotypes (Fig. 9, *A*, *B*, and *C*), with indistinguishable peak current amplitudes (instantaneous current measured at −145 mV [mean ± SEM, $n = 7$]: WT–D136G, 5.4 ± 1.0 μA; D136G–WT, 6.7 ± 1.2 μA; WT–D136G + D136G–WT, 6.6 ± 1.7 μA).

To quantitatively test for possible contributions of pure WT or pure D136G components in oocytes co-injected with WT–D136G and D136G–WT RNA, we examined the voltage dependence of I_{ss}/I_{peak} in oocytes expressing the three different channel populations (WT–D136G, WT–D136G + D136G–WT, and D136G–WT) (Fig. 9 *D*). In these experiments, I_{ss}/I_{peak} was measured during a series of test potentials from a holding potential of −30 mV. Expression of both heterotandems alone or in combination exhibit identical voltage dependencies of I_{ss}/I_{peak} that are distinct from that observed for pure WT and D136G currents. This observation rules out any contribution from diagonal vs. adjacent subunit arrangements making it highly unlikely that a tetrameric assembly of one WT–D136G and one D136G–WT give rises to current phenotypes as ob-

served in the cotransfection studies with WT–WT and D136–D136G. Therefore our co-expression studies provide strong evidence that hClC-1 forms functional dimers.

DISCUSSION

Discerning the oligomeric structure of voltage-gated ion channels continues to be an important but challenging area of investigation. Because of the difficulties applying structural approaches such as x-ray diffraction or electron microscopy to the study of ion channels, a variety of functional approaches have been developed. MacKinnon (1991) described a method in which co-expression of wild-type and charybdotoxin-insensitive mutant *Shaker* potassium channels in *Xenopus* oocytes helped to deduce the number of subunits per channel by means of a binomial analysis of the blocking action of the toxin. To avoid uncertainties regarding the expression of heterogenous RNA mixtures in oocytes, other investigators have chosen to construct cDNAs encoding artificial heteromultimeric potassium channels with fixed subunit stoichiometries to investigate oligomeric structure (Isacoff et al., 1990; Liman et al., 1992). It is now possible to apply a similar approach toward defining the subunit composition of mammalian voltage-gated ClC-type chloride channels. This is due to the availability of a mutant hClC-1 (D136G) having a well characterized functional phenotype that differs substantially from the WT channel (Fahlke et al., 1995).

Our data demonstrates that the heterodimeric WT–D136G construct encodes a homogenous population of channels with novel gating properties that cannot be explained by simple addition of the two separate WT and D136G phenotypes (Fig. 3). The functional homogeneity of the WT–D136G channel population is supported by the demonstration of monoexponential time course of current activation (Fig. 4, *A* and *B*). These findings are not consistent with the expression of a mixture of homomultimeric and heteromultimeric channels, and therefore rule out the possibility that homodimeric channels are formed in these experiments by misassembly of WT–D136G (channels formed by subunits contributed by more than one WT–D136G molecule). However, these data alone do not rule out that the channel complex is a tetramer.

Our cotransfection experiments using WT–WT and D136G–D136G help to rule out the possibility that the number of subunits per channel is greater than two. This is best appreciated by considering simple possible configurations of the two homodimeric channels as shown in Fig. 5 *B*. In the case of heterotetramer formation, we would expect three Cl⁻ channel phenotypes (WT, D136G, WT–D136G) to co-exist. What we observed fits best with a simple superimposition of the two WT and D136G current phenotypes (Fig. 7). We can-
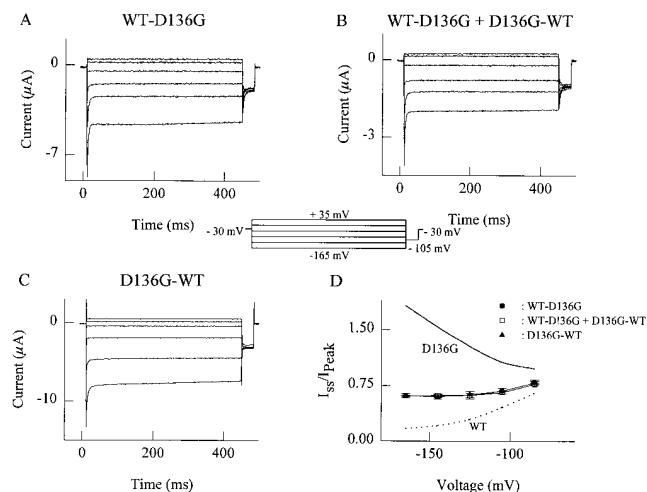

FIGURE 9.   Co-expression of heterotandem hClC-1 constructs in *Xenopus* oocytes. (*A*) Recordings from oocytes expressing WT–D136G. Currents were elicited by voltage steps from −165 to +35 mV in 40-mV steps from a holding potential of −30 mV. (*B*) Recordings from oocytes expressing D136G–WT. Currents were elicited by voltage steps from −165 to +35 mV in 40-mV steps from a holding potential of −30 mV. (*C*) Recordings made from oocytes expressing both WT–D136G and D136G–WT. (*D*) Plot of the fraction of steady-current (I_{ss}/I_{peak}) vs voltage obtained from four to five cells. Lines without data points represent averaged data plots for D136G (*solid line*, $n = 4$) and WT (*dotted line*, $n = 4$) determined under identical conditions in oocytes.

not completely exclude the possibility that WT–WT and D136G–D136G only interact to form homotetrameric pores or that heterotetramer formation is unstable in this experiment. However, preferential assembly of homomultimeric channels seems very unlikely in view of the highly efficient expression of both heterotandem constructs, and the lack of evidence for homomultimeric channels in WT–D136G transfected cells. Similarly, trimeric channels resulting from the assembly of one dimer molecule with a single subunit of a separate dimer molecule seems unlikely because of the homogeneity of channel expression with WT–D136G alone, and the absence of heteromultimeric channels in the homodimer co-transfection experiment.

Finally, we have excluded that a tetrameric assembly could be responsible for the expression of summed WT and D136G phenotypes uniquely in the homodimer co-expression experiments due to the adjacent arrangement of the subunits. To do this we examined the heterotandem constructs WT–D136G and D136G–WT together in *Xenopus* oocytes. This experiment was performed to rule out that adjacent (vs. diagonal) arrangement of hClC-1 subunits in a tetrameric complex might lead to a summed phenotype. As illustrated in Fig. 5 *C*, co-assembly of the two heterotandem channels will produce diagonal and adjacent complexes in a 2:1 ratio. If the adjacent configuration gives rise to the summed phenotype while the diagonal configurations result in channels that exhibit a mixed gating phenotype resembling WT–D136G alone, we should have observed a more complex gating behavior in cells co-expressing both heterotandems. The absence of such a complex gating phenotype and the identity of these results with those obtained with either heterotandem channel alone rules out cross-talk within the context of a tetrameric channel complex and indicates that only dimeric channels are functional.

In support of a dimeric structure for hClC-1, we have also presented biochemical evidence that the recombinant channel forms native complexes consistent with a two subunit structure. Sucrose density gradient centrifugation of triton X-100 solubilized membranes from hClC-1 expressing HEK-293 cells indicates that the molecular mass of the native channel ($\sim$158–240 kD) is close to twice the predicted mass of a single subunit ($\sim$120–130 kD). Furthermore, the sedimentation properties of hClC-1 are the same for proteins encoded by both monomeric and tandem cDNA constructs. Our results indicate a dimeric structure for hClC-1 when it is expressed heterologously. The size of the channel complex in native skeletal muscle should be similar unless additional non-identical subunits or cytoskeletal elements unique to muscle are incorporated.

Our conclusion that hClC-1 is a dimer conflicts with the previously published study by Steinmeyer et al. that infers a tetrameric structure of this channel from RNA titration experiments using two nonfunctional hClC-1 mutants (Steinmeyer et al., 1994). There are several issues that can be raised about this previous study that could explain this discrepancy. First, these experiments were performed in *Xenopus* oocytes and current recordings are subject to contamination with an endogenous calcium-activated Cl$^-$ channel. Second, the authors may have underestimated the extent of competition for expression by comparing mixtures of two different hClC-1 alleles with mixtures of hClC-1 with the cystic fibrosis transmembrane conductance regulator (CFTR). Because competition for expression is expected to depend upon the number of molecules competing for ribosomal engagement, use of CFTR (twice the molecular weight of hClC-1) contributes $\sim$50% less on an equal weight basis than would another hClC-1 allele (higher molar quantity). Finally, these experiments were performed with non-functional mutants and therefore these investigators are limited in their ability to evaluate the true proportion of expressed WT vs mutant channel proteins. This limitation raises some uncertainty as to the validity of their binomial analysis for determining subunit stoichiometry of hClC-1.

Middleton et al. (1994) discussed two fundamentally different quaternary architectures for the formation of two identical, but independently gated pores in the dimeric ClC-0 protein: either each ion pore is formed completely by one subunit (one pore/one subunit), or each subunit contributes to the formation of both protochannels (shared pore concept). The observation that WT–D136G forms a homogenous population of Cl$^-$ channels with novel gating properties raises interesting possibilities for the function of hClC-1. If each hClC-1 subunit encodes a complete ion pore, then there must be a single mechanism that gates both pores in the dimeric channel in an identical fashion. This is analogous to the slow gate of ClC-0, but in hClC-1 this gating mechanism has fast kinetics. Our results are not consistent with a separate mechanism that gates each protochannel separately. In other words, independent gating of two separate ion pores seems improbable based upon the results we obtained with WT–D136G. Additional studies, possibly exploiting the heterotandem strategy with a pore altering mutation, will be needed in the future to determine the true stoichiometry of the hClC-1 pore.

REFERENCES

Adachi, S., S. Uchida, H. Ito, M. Hata, M. Hiroe, F. Marumo, and S. Sasaki. 1994. Two isoforms of a chloride channel predominantly expressed in thick ascending limb of Henle's loop and collecting ducts of rat kidney. *J. Biol. Chem.* 269:17677–17683.

Bauer, C.K., K. Steinmeyer, J.R. Schwarz, and T.J. Jentsch. 1991. Completely functional double-barreled chloride channel expressed from a single *Torpedo* cDNA. *Proc. Natl. Acad. Sci. USA.* 88:11052–11056.

Chahine, M., A.L. George, Jr., M. Zhou, S. Ji, W. Sun, R.L. Barchi, and R. Horn. 1994. Sodium channel mutations in paramyotonia congenita uncouple inactivation from activation. *Neuron.* 12:281–294.

Deal, K.K., D.M. Lovinger, and M.M. Tamkun. 1994. The brain Kv1.1 potassium channel: in vitro and in vivo studies on subunit assembly and posttranslational processing. *J. Neurosci.* 14:1666–1676.

Fahlke, C., A. Rosenbohm, N. Mitrovic, A.L. George, Jr., and R. Rüdel. 1996. Mechanism of voltage-dependent gating in skeletal muscle chloride channels. *Biophys. J.* 71:695–706.

Fahlke, C., R. Rüdel, N. Mitrovic, M. Zhou, and A.L. George, Jr. 1995. An aspartic acid residue important for voltage-dependent gating of human muscle chloride channels. *Neuron.* 15:463–472.

Fisher, S.E., G.C. M. Black, S.E. Lloyd, E. Hatchwell, O. Wrong, R.V. Thakker, and I.W. Craig. 1994. Isolation and partial characterization of a chloride channel gene which is expressed in kidney and is a candidate for Dent's disease (an X-linked hereditary nephrolithiasis). *Hum. Mol. Genet.* 3:2053–2059.

Gurnett, C.A., S.D. Kahl, R.D. Anderson, and K.P. Campbell. 1995. Absence of the skeletal muscle sarcolemma chloride channel ClC-1 in myotonic mice. *J. Biol. Chem.* 270:9035–9038.

Hamill, O.P., A. Marty, E. Neher, B. Sakmann, and F.J. Sigworth. 1981. Improved patch-clamp techniques for high-resolution current recording from cells and cell-free membrane patches. *Pflüg. Arch.* 391:85–100.

Hanke, W., and C. Miller. 1983. Single chloride channels from *Torpedo* electroplax. Activation by protons. *J. Gen. Physiol.* 82:25–45.

Higuchi, R. 1989. Using PCR to engineer DNA. *In* PCR Technology. H.A. Erlich, editor. Stockton Press, New York. 61–70.

Isacoff, E.Y., Y.N. Jan, and L.Y. Jan. 1990. Evidence for the formation of heteromultimeric potassium channels in *Xenopus* oocytes. *Nature (Lond.).* 345:530–534.

Jentsch, T.J., K. Steinmeyer, and G. Schwarz. 1990. Primary structure of *Torpedo marmorata* chloride channel isolated by expression cloning in *Xenopus* oocytes. *Nature (Lond.).* 348:510–514.

Jentsch, T.J. 1994. Molecular biology of voltage-gated chloride channels. *Curr. Top. Membr.* 42:35–57.

Kawasaki, M., S. Uchida, T. Monkawa, A. Miyawaki, K. Mikoshiba, F. Maruma, and S. Sasaki. 1994. Cloning and expression of a protein kinase C-regulated chloride channel abundantly expressed in rat brain neuronal cells. *Neuron.* 12:597–604.

Kieferle, S., P. Fong, M. Bens, A. Vandewalle, and T.J. Jentsch. 1994. Two highly homologous members of the ClC chloride channel family in both rat and human kidney. *Proc. Natl. Acad. Sci. USA.* 91:6943–6947.

Liman, E.R., J. Tytgat, and P. Hess. 1992. Subunit stoichiometry of a mammalian K^+ channel determined by construction of multimeric cDNAs. *Neuron.* 9:861–871.

MacKinnon, R. 1991. Determination of the subunit stoichiometry of a voltage-activated potassium channel. *Nature (Lond.).* 350:232–235.

Malinowska, D.H., E.Y. Kupert, A. Bahinski, A.M. Sherry, and J. Cuppoletti. 1995. Cloning, functional expression, and characterization of a PKA-activated gastric Cl^- channel. *Am. J. Physiol.* 268:C191–C200.

McCormack, K., L. Lin, L.E. Iverson, M.A. Tanouye, and F.J. Sigworth. 1992. Tandem linkage of Shaker K^+ channel subunits does not ensure the stoichiometry of expressed channels. *Biophys. J.* 63:1406–1411.

Middleton, R.E., D.J. Pheasant, and C. Miller. 1994. Purification, reconstitution, and subunit composition of a voltage-gated chloride channel from *Torpedo* electroplax. *Biochemistry.* 33:13189–13198.

Miller, C. 1982. Open-state substructure of single chloride channels from *Torpedo* electroplax. *Philos. Trans. R. Soc. Lond. B Biol. Sci.* 299:401–411.

Miller, C., and M.M. White. 1984. Dimeric structure of single chloride channels from *Torpedo* electroplax. *Proc. Natl. Acad. Sci. USA.* 81:2772–2775.

Pusch, M., K. Steinmeyer, and T.J. Jentsch. 1994. Low single channel conductance of the major skeletal muscle chloride channel, ClC-1. *Biophys. J.* 66:149–152.

Steinmeyer, K., C. Ortland, and T.J. Jentsch. 1991. Primary structure and functional expression of a developmentally regulated skeletal muscle chloride channel. *Nature (Lond.).* 354:301–304.

Steinmeyer, K., C. Lorenz, M. Pusch, M.C. Koch, and T.J. Jentsch. 1994. Multimeric structure of ClC-1 chloride channel revealed by mutations in dominant myotonia congenita. *EMBO (Eur. Mol. Biol. Organ.) J* 13:737–743.

Thiemann, A., S. Grunder, M. Pusch, and T.J. Jentsch. 1992. A chloride channel widely expressed in epithelial and non-epithelial cells. *Nature (Lond.).* 356:57–60.

Uchida, S., S. Sasaki, T. Furukawa, M. Hiraoka, T. Imai, Y. Hirata, and F. Marumo. 1993. Molecular cloning of a chloride channel that is regulated by dehydration and expressed predominantly in kidney medulla. *J. Biol. Chem.* 268:3821–3824.

van Siegtenhorst, M.A., M.T. Bassi, G. Borsani, M.C. Wapenaar, G.B. Ferrero, L. de Concillis, E.I. Rugarli, A. Grillo, B. Franco, H.Y. Zoghbi, and A. Ballabio. 1994. A gene from the Xp22.3 region shares homology with voltage-gated chloride channels. *Hum. Mol. Genet.* 3:547–552.